Backpropagation-Free Test-Time Adaptation for Lightweight EEG-Based Brain-Computer Interfaces

Siyang Li, Jiayi Ouyang, Zhenyao Cui, Ziwei Wang, Tianwang Jia, Feng Wan, and Dongrui Wu, *Fellow, IEEE*

Abstract—Electroencephalogram (EEG)-based brain-computer interfaces (BCIs) face significant deployment challenges due to inter-subject variability, signal non-stationarity, and computational constraints. While test-time adaptation (TTA) mitigates distribution shifts under online data streams without per-use calibration sessions, existing TTA approaches heavily rely on explicitly defined loss objectives that require backpropagation for updating model parameters, which incurs computational overhead, privacy risks, and sensitivity to noisy data streams. This paper proposes Backpropagation-Free Transformations (BFT), a TTA approach for EEG decoding that eliminates such issues. BFT applies multiple sample-wise transformations of knowledge-guided augmentations or approximate Bayesian inference to each test trial, generating multiple prediction scores for a single test sample. A learning-to-rank module enhances the weighting of these predictions, enabling robust aggregation for uncertainty suppression during inference under theoretical justifications. Extensive experiments on five EEG datasets of motor imagery classification and driver drowsiness regression tasks demonstrate the effectiveness, versatility, robustness, and efficiency of BFT. This research enables lightweight plug-and-play BCIs on resource-constrained devices, broadening the real-world deployment of decoding algorithms for EEG-based BCI.

Index Terms—Brain-computer interface, domain adaptation, electroencephalogram, test-time adaptation, transfer learning

I. INTRODUCTION

BRAIN-COMPUTER interfaces (BCIs) translate neural activity into control commands that enable direct interaction between users and external systems. BCI systems support cognitive and sensorimotor assistance, and are increasingly evolving toward closed-loop platforms for neurorehabilitation and cognitive enhancement [1]. Non-invasive BCIs, which typically rely on electroencephalography (EEG) sensors, remain the most accessible.

EEG-based BCIs are commonly applied in motor imagery (MI), wherein users mentally rehearse limb movements to activate motor cortical regions [2]. The resulting EEG signals are decoded in real time into discriminative control commands for devices such as prosthetics, exoskeletons, or computer cursors. Beyond active control, EEG also enables passive BCIs for cognitive-state monitoring, e.g., emotion recognition [3], and driver drowsiness estimation [4]. In such applications, EEG reflects variations in mental status, with real-time monitoring offering substantial benefits for safety-critical tasks such as driving.

Despite being surgery-free and relatively low cost, EEG signals suffer from high inter-subject variability and nonstationarity. EEG responses can vary significantly between users and even across sessions for the same user, due to fluctuations in mental state, concentration, or electrode contact quality [5]. Consequently, most EEG decoding algorithms require lengthy calibration sessions before each use, limiting their practicality in real-world deployments.

Transfer learning (TL) [6] offers a promising direction to reduce or eliminate calibration by leveraging auxiliary data from additional subjects. While classic TL assumes an offline transductive setting, test-time adaptation (TTA) [7], [8] supports a more practical online setting where models adapt sequentially to streaming test data. TTA is particularly well-suited for real-time applications, enabling better decoding algorithms for plug-and-play BCIs that are calibration-free.

Although recent TTA methods enable plug-and-play EEG decoding with promising accuracy [9], their real-world applicability remains limited. Challenges include the computational cost of backpropagation, the need for white-box access to model parameters, susceptibility to noise, and limitations to classification tasks. As illustrated in Fig. 1, these constraints suggest the urgent need for backpropagation-free, privacy-preserving, noise-robust, and task-agnostic TTA approaches.

This paper introduces a Backpropagation-Free Transformation (BFT) approach for online TTA in EEG-based BCIs, particularly under deployment scenarios with constrained computational resources. BFT applies sample-wise transformations to each test sample and aggregates predictions across these variants to implicitly reduce inference uncertainty. To further differentiate across the representations of transformations, a learning-to-rank module prioritizes the more reliable transformations for inference aggregation. By relying solely on forward propagation, BFT achieves lightweight adaptation. Extensive experiments on three MI classification and two driver-drowsiness regression EEG datasets demonstrate that BFT is much more practical than current TTA approaches.

Our main contributions are summarized as follows:

1) Proposal of BFT, a lightweight TTA approach that is backpropagation-free, privacy-preserving, noise-robust, and task-agnostic.
2) Theoretical justification of BFT, on the aggregation of predictions to test-time transformations.

S. Li, J. Ouyang, Z. Cui, Z. Wang, T. Jia, and D. Wu are with the Ministry of Education Key Laboratory of Image Processing and Intelligent Control, School of Artificial Intelligence and Automation, Huazhong University of Science and Technology, Wuhan 430074, China. They are also with the Shenzhen Huazhong University of Science and Technology Research Institute, Shenzhen, China.

F. Wan is with the Department of Electrical and Computer Engineering, Faculty of Science and Technology, University of Macau, Macau 999078, China, and also with the Centre for Cognitive and Brain Sciences, Institute of Collaborative Innovation, University of Macau, Macau 999078, China.

S. Li, J. Ouyang, and Z. Cui contributed equally to this work.

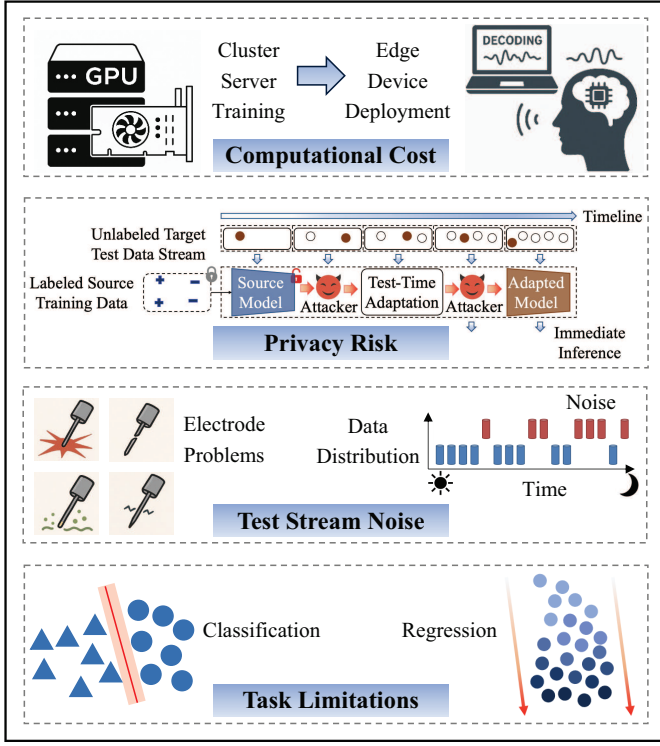Corresponding Author: Dongrui Wu (drwu09@gmail.com).

Fig. 1. Key issues in deploying TTA algorithms for BCI decoding.

3) Experiments under practical scenarios of real-time inference and test-time noise, verifying the effectiveness, versatility, robustness, and efficiency of BFT.

4) Demonstration that high-performance online decoding algorithms can be deployed in plug-and-play EEG-based BCIs without per-use calibration, thereby improving usability and broadening application potential.

The remainder of this paper is organized as follows: Section II introduces related work. Section III proposes BFT. Section IV provides theoretical justification for BFT. Section V presents experimental results to demonstrate the performance of BFT. Finally, Section VI concludes and points out some future research directions.

II. RELATED WORKS

This section reviews TTA approaches. TL approaches for unsupervised domain adaptation (UDA) restricted to offline transductive analysis have been comprehensively discussed by Li *et al.* [9] and are thus omitted. Such approaches are compared in the experiments solely to demonstrate offline TL capabilities.

A. Transfer Learning

Conventional machine learning assumes that training and test sets are independently and identically distributed (i.i.d.), drawn from the same underlying distribution. TL [6] relaxes this assumption by leveraging knowledge from the source domain to improve performance on the target domain under distribution shift. This field of study is also known as domain adaptation [6] or concept drift [10].

TL typically addresses three types of distribution shift:

1) **Marginal Distribution Shift:** $P_s(\mathbf{x}) \neq P_t(\mathbf{x})$, i.e., changes in the input distribution.
2) **Conditional Distribution Shift:** $P_s(y|\mathbf{x}) \neq P_t(y|\mathbf{x})$, i.e., changes in the prediction function.
3) **Label Distribution Shift:** $P_s(y) \neq P_t(y)$, i.e., changes in class priors.

B. Test-Time Adaptation

In real-time BCIs, test samples arrive sequentially and require low-latency inferences. As a result, the classic UDA setting is inapplicable. TTA [7], [8], [11] provides a more practical alternative and can be viewed as a constrained form of UDA, characterized by:

1) No access to source data; only the pretrained source model is available. This is the key distinction between source-free UDA and vanilla UDA, and it also applies to the TTA setting in general.
2) Access restricted to a small subset of unlabeled target samples at any given time.
3) Iterative optimization is avoided due to computational constraints.

The representative TTA approaches are summarized and categorized in the following paragraphs:

TTA for Mitigating Marginal Distribution Shift. Batch Normalization test-time adaptation (BN-adapt) [12] is the most straightforward approach. Test entropy minimization (Tent) [13] also updates the batch normalization layers, but through minimizing the entropy of model predictions on test inputs using backpropagation. For EEG data, Euclidean Alignment (EA) [14] normalizes the mean covariance matrices of each domain to the identity matrix, and Li *et al.* [9] showed that EA can be seamlessly applied to TTA, with an online updated target reference matrix.

TTA for Mitigating Conditional Distribution Shift. Target Pseudo-Labels (PL) [15] is the most straightforward approach. Uncertainty minimization is an extremely effective measure for implicit mitigation of conditional distribution shift. Sharpness-aware and reliable entropy minimization (SAR) [16] selects samples with smaller entropy losses and jointly minimizes the sharpness of the entropy and the entropy loss for a more reliable adaptation. Test-Time Information Maximization Ensemble (T-TIME) [9] extends the information maximization loss objective, which incorporates an additional uniform regularization of label distribution into classic conditional entropy, to TTA.

TTA for Mitigating Label Distribution Shift. Label shift is a difficult problem, and often has to resort to pseudo-labels for estimating statistics of the target label distribution. Marginal Entropy Minimization with One test point (MEMO) [17] regularizes the model to produce similar predictions for each transformation through mean entropy minimization. Li *et al.* [9] incorporated label shift into information maximization through online estimation.

C. Test-Time Adaptation Beyond Model Update

Despite recent advances in decoding performance [9], deploying TTA algorithms in BCIs remains challenging due to several practical constraints.

Computational Cost. TTA approaches often rely on loss objectives under backpropagation, which is infeasible on low-power BCI devices lacking dedicated GPUs. Such an issue is exacerbated by model quantization [18], such as converting EEGNet from 32-bit to 8-bit integers for deployment [19], which hinders retraining or fine-tuning with backpropagation.

Privacy Risk. Updating model parameters during inference requires access to internal weights, exposing sensitive information. Black-box deployment is much more preferable for preserving model privacy [20], [21].

Test Stream Noise. EEG is highly susceptible to artifacts caused by fatigue, movement, sweat, poor electrode contact, etc. Such noise increases the difficulties of hyperparameter selection, model selection, and the combination of different types of shifts for TTA approaches [22], which could lead to negative transfer when not appropriately handled [23].

Task Limitations. Most TTA approaches, and TL approaches more broadly, are designed for classification and rely on predicted class probabilities, which restricts their applicability to regression tasks. Approaches that address conditional or label distribution shifts in regression remain largely unexplored.

These limitations highlight the urgent need for a TTA framework that is backpropagation-free, privacy-preserving, noise-robust, and task-agnostic. While a few recent methods remove the need for backpropagation, they offer limited gains and remain unsuitable for regression.

III. BACKPROPAGATION-FREE TRANSFORMATIONS FOR TEST-TIME ADAPTATION

This section presents the proposed BFT method, which enables TTA without requiring access to model parameters, gradients, or batched inputs during inference.

A. Problem Formulation

Let $\mathcal{D}_{\text{test}} = \{\mathbf{x}_t\}_{t=1}^{n_t}$ denote a streaming test set, where $\mathbf{x}_t$ is a test input. The deployed model comprises a feature extractor $g(\cdot)$ and a task-specific classifier or regressor $h(\cdot)$, trained on a training set $\mathcal{D}_{\text{train}} = \{(\mathbf{x}_i, y_i)\}_{i=1}^{n_s}$, which is assumed to be unavailable at test time.

Due to distributional shifts between the source and target domains (e.g., across subjects or sessions), model performance may degrade at test time. TTA addresses this degradation by refining predictions during online inference. At each time step t, TTA aims to improve the prediction $\hat{y}_t$ based on $\{\mathbf{x}_t, \hat{y}_t, g, h\}$.

B. Test-Time Transformations

Uncertainty estimation is widely employed in TL, particularly to implicitly address conditional distribution shifts beyond marginal distribution shifts. Shannon entropy, derived from the softmax output of a classifier, serves as a representative: high entropy indicates domain mismatch, while low entropy suggests alignment. However, entropy minimization necessitates backpropagation and is therefore inapplicable in backpropagation-free settings or regression tasks.

To overcome this limitation, we propose test-time transformations that can be considered as structured perturbations. Intuitively, if a model is well-aligned to the target domain, its predictions should remain stable under such perturbations. Thus, the variability of predictions across transformed inputs can be used as a surrogate measure of uncertainty. A more detailed theoretical derivation is offered in Section IV.

We consider two types of transformations, with illustrations shown in Fig. 2.
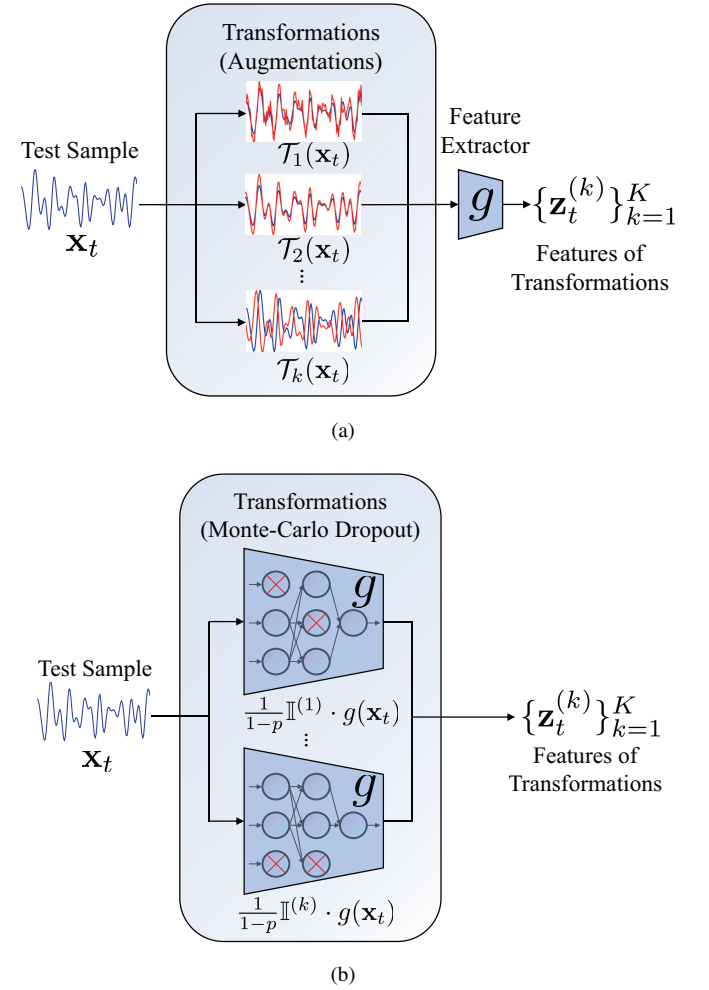

(a)

(b)

Fig. 2. Two types of transformations. (a) BFT-A; and (b) BFT-D.

Knowledge-guided Augmentations (referred to as BFT-A): These transformations are commonly employed for EEG data augmentation [24]:

1) *Noise Addition (Noise):* Injects uniform noise into the input signal.
2) *Amplitude Scaling (Scale):* Multiplies the signal by a scalar close to one to slightly adjust its amplitude.
3) *Frequency Shift (Freq):* Uses the Hilbert transform to shift the signal's frequency content.

4) *Sliding Window (Slide):* Generates overlapping temporal segments from each trial using a sliding window.

Such augmentations are a set of K deterministic or stochastic transformations, denoted as $\{\mathcal{T}_k(\cdot)\}_{k=1}^K$, applied to input $\mathbf{x}_t$. The resulting features of each of the transformations are:

$$\mathbf{z}_t^{(k)} = g(\mathcal{T}_k(\mathbf{x}_t)). \tag{1}$$

Approximate Bayesian Inference via Monte-Carlo Dropout (referred to as BFT-D): Dropout, typically disabled at test time, is reactivated to enable stochastic forward passes via Monte Carlo (MC) sampling [25].

Assuming that a dropout layer exists after $g(\cdot)$, each transformation employs a binary mask $\mathbb{I}^{(k)} \in \{0,1\}^d$ applied to the feature vector $g(\mathbf{x}_t) \in \mathbb{R}^d$. While dropout masks are commonly sampled from a Bernoulli distribution, in our approach, each mask deterministically drops a fixed subset of features to ensure consistency, which is essential for the ranking module introduced in the following subsection. Its values are:

$$\mathbb{I}_i^{(k)} = \begin{cases} 0, & \text{if } i \in \left[(k-1)\frac{d}{K},\ k\frac{d}{K}\right), \\ 1, & \text{otherwise,} \end{cases} \tag{2}$$

where $\frac{1}{K}$ corresponds to the original training-time dropout rate p. Different masks would thus generate different subsets of features of the same test sample. Note that features can also be dropped non-consecutively, and can also have overlaps across masks.

The resulting feature of each of the transformations is:

$$\mathbf{z}_t^{(k)} = \frac{1}{1-p}\mathbb{I}^{(k)} \cdot g(\mathbf{x}_t), \tag{3}$$

where the scaling factor $\frac{1}{1-p}$ compensates for the reduced activation magnitude, thereby preserving the expected value of the feature vector under the masking, similar to that of training-time dropout.

Note that BFT-A modifies input data, whereas BFT-D alters features. Although both BFT-A and BFT-D require forward passes of multiple samples instead of the original test sample, both are computationally efficient due to batched forward passes under matrix operations. The original test sample's feature may also be included, as the identity transformation.

The representations of the transformations $\{\mathbf{z}_t^{(k)}\}_{k=1}^K$ are then forwarded through $h(\cdot)$ to produce multiple predictions for the same test sample $\mathbf{x}_t$.

C. Learning-to-Rank Transformations

Not all transformations produce equally reliable predictions. Simple aggregation schemes that assign uniform weights to all transformed outputs fail to account for the varying reliability levels of each transformation. To address this, we propose estimating reliability scores for each transformed input to enable a weighted combination. Inspired by learning-to-rank approaches [26], we further introduce a ranking-based strategy.

Consider a neural network module for ranking that receives feature representations from $g(\cdot)$ and outputs a scalar reliability score in a continuous space, analogous to a regression

model. This ranking module, denoted as $r(\cdot)$, can be built on the transformations of training samples. Naïvely, the reliability scores of these transformations can be simply based on the task losses, obtained using the trained classifier/regressor $h(\cdot)$. However, task losses alone are suboptimal for modeling transformation reliability due to several limitations:

- No additional information is introduced; $r(\cdot)$ merely replicates/distills the knowledge embedded in $h(\cdot)$.
- The loss values are typically close in magnitude since $h(g(\cdot))$ is optimized on the training data, thereby impeding the effective optimization of $r(\cdot)$.
- Lower task loss values would correspond to higher reliability, which is inversely correlated.
- Most importantly, Task losses ignore the relative relationship across different transformations of the same instance.

To address these challenges, $r(\cdot)$ must output positively correlated reliability scores that ideally resemble discrete rankings. To this end, we adopt a learning-to-rank strategy [27] by introducing an auxiliary mapping module $m(\cdot)$, which transforms the task loss after Softmax normalization scores in $[0,1]$ space into a pseudo-discrete space $[1, 2, \ldots, K]$ representing rank-like values. Illustrations are shown in Fig. 3. Although $m(\cdot)$ produces continuous outputs, this transformation effectively amplifies the separation between similar reliability scores, thereby facilitating more accurate modeling of transformation quality.
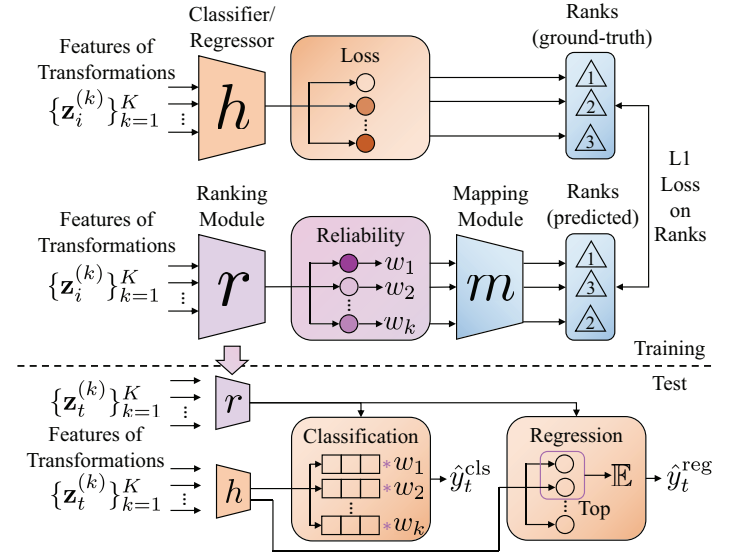

Fig. 3. Training and inference of the ranking module, and prediction aggregation strategy for classification and regression tasks, respectively.

Specifically, the mapping module $m(\cdot)$ is a light model that can be easily pre-trained on synthetic data. We followed [27] to generate synthetic samples $\mathcal{D}_{\text{synthetic}} = \{\tilde{\mathbf{x}}_i\}_{i=1}^{n_{\text{syn}}}$. Each synthetic sample is a vector $\tilde{\mathbf{x}}_i \in \mathbb{R}^K$ where each value of it is a randomly generated scalar $\tilde{x}_{i,k} \in [0,1]$. Its corresponding ground-truth rank vector is then $\tilde{\boldsymbol{\pi}}_i \in \mathbb{R}^K$ where each value is $\tilde{\pi}_{i,k} \in \{1, 2, \ldots, K\}$. The optimization objective for $m(\cdot)$ is $L1$ loss, which is a standard metric for comparing two

rankings:

$$\mathcal{L}_{\text{mapping}}[m(\cdot)] = \mathbb{E}_{\tilde{\mathbf{x}}_i \sim \mathcal{D}_{\text{synthetic}}} \left\| m(\tilde{\mathbf{x}}_i) - \tilde{\boldsymbol{\pi}}_i \right\|_1. \quad (4)$$

Note that the input and output spaces of the mapping modules are continuous, instead of discrete. This mapping module thus avoids non-differentiable projection into the ranking space.

After optimizing the mapping module $m(\cdot)$, the ranking module $r(\cdot)$ is trained using the training set $\{\mathbf{x}_i\}_{i=1}^{n_s}$. It takes features of transformations $\{\mathbf{z}_i^{(k)}\}_{k=1}^K$ from the pre-trained feature extractor $g(\cdot)$ as inputs, and outputs reliability scores. The mapping module then projects such scores into ranks. The ground-truth rank vector for the ranking of the transformations for a specific sample is determined by the task module.

Specifically, the outputs of the ranking module $r(\cdot)$ first go through a Softmax function to convert into the weight vector $\mathbf{w}_i \in \mathbb{R}^K$ of values $w_{i,k}$ that sum up to one:

$$w_{i,k} = \frac{\exp\left(r(\mathbf{z}_i^{(k)})\right)}{\sum_{j=1}^K \exp\left(r(\mathbf{z}_i^{(j)})\right)}. \quad (5)$$

The loss objective is therefore still a regression $L1$ loss in the integer-like space:

$$\mathcal{L}_{\text{ranking}}[r(\cdot)] = \mathbb{E}_{\mathbf{x}_i \sim \mathcal{D}_{\text{train}}} \left\| m(\mathbf{w}_i) - \boldsymbol{\pi}_i \right\|_1. \quad (6)$$

To summarize, by decoupling transformation ranking from direct supervision via task loss, the learnable ranking module amplifies the distinction of reliability levels across transformations, handling the aforementioned limitations.

D. Inference Aggregation

To aggregate the predictions to the multiple transformations, we define the following strategies:

- **Classification:** The core concept of ensemble for classification can be regarded as applying higher weights to more reliable predictions for a convex combination [28]. The classifier's logit outputs $h(\mathbf{z}_t^{(k)})$ are first sharpened using temperature rescaling, a standard technique for adjusting the confidence of predictions prior to applying the Softmax function. The sharpened logits are then transformed into class probabilities via the Softmax function and aggregated using the reliability scores as weights from the ranking module $r(\cdot)$:

$$\hat{y}_t^{\text{cls}} = \underset{c \in \{1,...,C\}}{\arg\max} \left[\sum_{k=1}^K w_{t,k} \frac{\exp\left(\left[h(\mathbf{z}_t^{(k)})\right]_c / \tau\right)}{\sum_{c'=1}^C \exp\left(\left[h(\mathbf{z}_t^{(k)})\right]_{c'} / \tau\right)} \right], \quad (7)$$

where C denotes the number of classes, $w_{t,k}$ the reliability scores, and τ is the temperature hyperparameter. The value of τ is typically a power of two and less than one to ensure sharpening of the probability distribution.

- **Regression:** For regression tasks, the weight-based aggregation strategy is not applicable since outputs are continuous scalar values rather than probability distributions. Therefore, we instead average the predictions from the

top-ranked half of the transformations, as determined by the reliability scores from the ranking module $r(\cdot)$. Let k_j' denote the index of the transformation with the j-th highest value of $r(\mathbf{z}_t^{(k)})$. The aggregated prediction is then given by:

$$\hat{y}_t^{\text{reg}} = \frac{1}{\left\lceil \frac{K}{2} \right\rceil} \sum_{j=1}^{\left\lceil \frac{K}{2} \right\rceil} h(\mathbf{z}_t^{(k_j')}), \quad (8)$$

where $\lceil \cdot \rceil$ denotes the ceiling operator.

E. Summary of BFT

The pseudo-code for BFT is presented in Algorithm 1.

In summary, BFT reduces prediction uncertainty at the instance level, thereby implicitly addressing conditional distribution shifts, achieving gains similar to classic TL on uncertainty mitigation. Compared to classic approaches, BFT is backpropagation-free, privacy-preserving, noise-robust, and supports both classification and regression tasks. To address marginal distribution shifts, existing techniques such as EA [9], [14] and BN-adapt [12] are effective and fully compatible with BFT, without conflicting with the core properties.

IV. THEORETICAL FOUNDATION FOR BFT

This section gives a variance-based justification for BFT. We show that aggregating multiple stochastic test-time predictions can reduce prediction uncertainty, yielding more stable outputs and better transferability under domain shift.

A. Label-Preserving Test-Time Randomization

Definition 1 (Test-Time Randomization and Aggregation). *Let ζ denote the test-time randomness used to produce a prediction (e.g., a sampled label-preserving transform in BFT-A, or a dropout/mask draw in BFT-D). Fix an input $\mathbf{x}$. Define the scalar prediction under ζ as*

$$f(\zeta; \mathbf{x}) := \mathbb{E}[y|\mathbf{x}; \zeta] \in \mathbb{R}, \quad (9)$$

where the expectation is taken with respect to the model-induced predictive distribution.

To quantify the variability of the prediction induced by the stochasticity of ζ, single-shot test-time uncertainty is measured via the variance:

$$V_0 := \text{Var}_\zeta\big(f(\zeta; \mathbf{x})\big). \quad (10)$$

Draw $\zeta_1, \ldots, \zeta_K$ and set $f_k := f(\zeta_k; \mathbf{x})$. The k-th draw defines the k-th test-time branch (one stochastic transformation or one sampled dropout mask forward pass). In the basic case $\zeta_1, \ldots, \zeta_K$ are independently and identically distributed (i.i.d.); more generally we allow $\zeta_k \sim \mathcal{A}_k$ with branch-specific distributions $\{\mathcal{A}_k\}_{k=1}^K$.

A learning-to-rank module outputs weights $\mathbf{w} = (w_1, \ldots, w_K)$ with $w_k \geq 0$ and $\sum_{k=1}^K w_k = 1$, and the aggregation is

$$\hat{f}_{\mathbf{w}}(\mathbf{x}) := \sum_{k=1}^K w_k f_k. \quad (11)$$

Algorithm 1: Backpropagation-Free Transformations (BFT)

Input: Streaming test data $\{\mathbf{x}_t\}_{t=1}^{n_t}$;
  Labeled training data $\{(\mathbf{x}_i, y_i)\}_{i=1}^{n_s}$;
  $g(\cdot)$, the trained feature extractor;
  $h(\cdot)$, the trained classifier or regressor;
  $r(\cdot)$, the ranking module;
  $m(\cdot)$, the mapping module;
  K, the number of transformations;
  $\{\mathcal{T}_k(\cdot)\}_{k=1}^{K}$, the knowledge-guided transformation functions for BFT-A;
  τ, the temperature rescaling factor;
Output: Prediction $\hat{y}_t^{\text{cls}}$ or $\hat{y}_t^{\text{reg}}$ for each $\mathbf{x}_t$;
  // Mapping Module Training
  Generate $\mathcal{D}_{\text{synthetic}} = \{\tilde{\mathbf{x}}_i\}_{i=1}^{n_{\text{syn}}}$;
  Compute ground-truth ranks $\{\tilde{\pi}_i\}_{i=1}^{n_{\text{syn}}}$ for synthetic samples;
  Train m using $\mathcal{L}_{\text{mapping}}$ by Eq. (4);
  // Ranking Module Training
  Calculate transformed features $\{\mathbf{z}_i^{(k)}\}_{i=1,k=1}^{n_s,K}$ using training data $\{\mathbf{x}_i\}_{i=1}^{n_s}$, by Eq. (1) for BFT-A, or by Eq. (2) and Eq. (3) for BFT-D;
  Compute ranking weights $\{w_{i,k}\}_{i=1}^{n_s}$ using Eq. (5);
  Compute task-based rank labels $\{\pi_i\}_{i=1}^{n_s}$;
  Train r using $\mathcal{L}_{\text{ranking}}$ by Eq. (6);
  // Online Test Phase
  for $t = 1$ to n_t **do**
    Calculate transformed features $\{\mathbf{z}_t^{(k)}\}_{k=1}^{K}$ using test input $\mathbf{x}_t$, by Eq. (1) for BFT-A, or by Eq. (2) and Eq. (3) for BFT-D;
    if classification **then**
      Compute classification prediction $\hat{y}_t^{\text{cls}}$ by Eq. (7);
    else if regression **then**
      Compute regression prediction $\hat{y}_t^{\text{reg}}$ by Eq. (8)
    end if
  end for

The following deduction considers the naïve case where the learning-to-rank module considers a test input $\mathbf{x}$ and treats the realized weight vector $\mathbf{w}$ as deterministic. All variances are taken with respect to the joint randomness $(\zeta_1, \ldots, \zeta_K)$.

B. Variance Decomposition for Weighted Aggregation

Lemma 1 (Exact Variance Decomposition). *Fix an input $\mathbf{x}$. Let $f_k := f(\zeta_k; \mathbf{x})$ be square-integrable random variables induced by the joint test-time randomness, and define $\mu_k := \mathbb{E}[f_k]$ for $k = 1, \ldots, K$. Let $\hat{f}_{\mathbf{w}} := \sum_{k=1}^{K} w_k f_k$ with deterministic weights $\mathbf{w}$. Then we obtain*

$$\operatorname{Var}\left(\hat{f}_{\mathbf{w}}\right) = \sum_{k=1}^{K} w_k^2 \operatorname{Var}(f_k) + \sum_{i \neq j} w_i w_j \operatorname{Cov}(f_i, f_j). \quad (12)$$

Proof.

$$\operatorname{Var}(\hat{f}_{\mathbf{w}}) = \mathbb{E}\left[\left(\hat{f}_{\mathbf{w}} - \mathbb{E}[\hat{f}_{\mathbf{w}}]\right)^2\right] = \mathbb{E}\left[\left(\sum_{k=1}^{K} w_k(f_k - \mu_k)\right)^2\right]$$

$$= \sum_{i=1}^{K} \sum_{j=1}^{K} w_i w_j \, \mathbb{E}[(f_i - \mu_i)(f_j - \mu_j)]$$

$$= \sum_{i=1}^{K} \sum_{j=1}^{K} w_i w_j \operatorname{Cov}(f_i, f_j),$$

which yields (12) by separating diagonal and off-diagonal terms.

C. Homogeneous Variance Case

Assumption 1 (Homogeneous Prediction Variance). *Assume*

$$\operatorname{Var}(f_k) = \sigma^2, \qquad k = 1, \ldots, K. \quad (13)$$

If $\sigma^2 = 0$, the prediction is deterministic and variance reduction is trivial; otherwise the correlations defined below are well-defined.

Theorem 1 (Uncertainty Reduction under Homogeneous Variance). *Define $\rho_{ij} := \operatorname{Corr}(f_i, f_j)$ for $i \neq j$. Under Assumption 1,*

$$\operatorname{Var}\left(\hat{f}_{\mathbf{w}}(\mathbf{x})\right) = \sigma^2 \sum_{k=1}^{K} w_k^2 + \sigma^2 \sum_{i \neq j} w_i w_j \rho_{ij}. \quad (14)$$

Let

$$\rho_{\max} := \max_{\substack{i \neq j \\ i,j \in \{1, \ldots, K\}}} |\rho_{ij}| \in [0, 1]. \quad (15)$$

Then

$$\operatorname{Var}\left(\hat{f}_{\mathbf{w}}(\mathbf{x})\right) \leq \sigma^2\left(\rho_{\max} + (1 - \rho_{\max}) \sum_{k=1}^{K} w_k^2\right) \leq \sigma^2. \quad (16)$$

Moreover, $\operatorname{Var}(\hat{f}_{\mathbf{w}}(\mathbf{x})) < \sigma^2$ whenever $\rho_{\max} < 1$ and $\sum_{k=1}^{K} w_k^2 < 1$.

Proof. By Lemma 1 and Assumption 1, $\operatorname{Cov}(f_i, f_j) = \rho_{ij}\sigma^2$ for $i \neq j$, which gives (14). For the bound, use $|\rho_{ij}| \leq \rho_{\max}$ and $\sum_{i \neq j} w_i w_j = 1 - \sum_k w_k^2$:

$$\sum_{i \neq j} w_i w_j \rho_{ij} \leq \sum_{i \neq j} w_i w_j |\rho_{ij}| \leq \rho_{\max}\left(1 - \sum_{k=1}^{K} w_k^2\right),$$

where we used $(\sum_k w_k)^2 = 1 = \sum_k w_k^2 + \sum_{i \neq j} w_i w_j$. Substituting into (14) yields (16).

An illustrative visualization of Theorem 1 is provided in Fig. 4.

D. Heterogeneous Variance Case

In the heterogeneous-variance setting, the ensemble uncertainty is mainly affected by three factors: the worst-branch noise κ, the similarity between branches $\rho_{\max}$, and how spread the weights are K_{eff}.
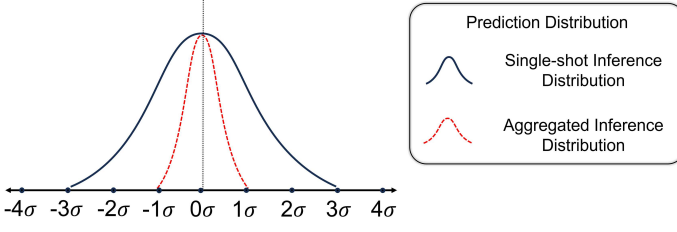
Fig. 4. Illustration of uncertainty reduction achieved through test-time transformations under the homogeneous variance assumption.

Assumption 2 (Heterogeneous Prediction Variance). *Fix an input* $\mathbf{x}$. *In the k-th branch (defined in Definition 1), the prediction f_k has heterogeneous variance:*

$$\mathrm{Var}(f_k) = \sigma_k^2, \qquad 0 < \sigma_k^2 \le \sigma_{\max}^2 < \infty, \quad k = 1, \ldots, K. \tag{17}$$

Consider $V_0 := \mathrm{Var}_\zeta\big(f(\zeta; \mathbf{x})\big)$ the single-shot test-time variance defined in (10), ζ follows the randomization used in single-shot inference. Assume that the worst branch variance is controlled relative to V_0:

$$\sigma_{\max}^2 \le \kappa V_0, \qquad 1 \le \kappa. \tag{18}$$

Theorem 2 (Uncertainty Reduction under Heterogeneous Variance). *Let $\rho_{\max}$ be defined in (15). Under Assumption 2, for any probability weights $\mathbf{w}$ (i.e., $w_k \ge 0$ and $\sum_{k=1}^K w_k = 1$),*

$$
\mathrm{Var}\big(\hat{f}_{\mathbf{w}}(\mathbf{x})\big) \le \sigma_{\max}^2\Big(\rho_{\max} + (1 - \rho_{\max})\sum_{k=1}^K w_k^2\Big)
$$

$$
\le \kappa V_0\Big(\rho_{\max} + (1 - \rho_{\max})\sum_{k=1}^K w_k^2\Big). \tag{19}
$$

Define the effective number of branches

$$K_{\mathrm{eff}} := \frac{1}{\sum_{k=1}^K w_k^2} \in [1, K]. \tag{20}$$

If $\rho_{\max} < 1/\kappa$, then a sufficient condition for $\mathrm{Var}\big(\hat{f}_{\mathbf{w}}(\mathbf{x})\big) < V_0$ is

$$K_{\mathrm{eff}} > \frac{\kappa(1 - \rho_{\max})}{1 - \kappa\rho_{\max}}. \tag{21}$$

Proof. For $i \ne j$, let $\rho_{ij} := \mathrm{Corr}(f_i, f_j)$. Then

$$
|\mathrm{Cov}(f_i, f_j)| = |\rho_{ij}|\sqrt{\mathrm{Var}(f_i)\mathrm{Var}(f_j)}
$$

$$
\le \rho_{\max}\sqrt{\sigma_i^2 \sigma_j^2} \le \rho_{\max}\sigma_{\max}^2. \tag{22}
$$

Since $w_i w_j \ge 0$,

$$
\sum_{i \ne j} w_i w_j \, \mathrm{Cov}(f_i, f_j) \le \rho_{\max}\sigma_{\max}^2 \sum_{i \ne j} w_i w_j
$$

$$
= \rho_{\max}\sigma_{\max}^2\Big(1 - \sum_{k=1}^K w_k^2\Big), \tag{23}
$$

where we used $\big(\sum_k w_k\big)^2 = 1 = \sum_k w_k^2 + \sum_{i \ne j} w_i w_j$. Moreover,

$$
\sum_{k=1}^K w_k^2 \mathrm{Var}(f_k) = \sum_{k=1}^K w_k^2 \sigma_k^2 \le \sigma_{\max}^2 \sum_{k=1}^K w_k^2. \tag{24}
$$

Combining (23) and (24) with (12) yields the first inequality in (19). The second inequality follows from (18).

For the sufficient condition, it is enough to ensure that the upper bound in (19) is strictly smaller than V_0, namely

$$
\kappa\Big(\rho_{\max} + (1 - \rho_{\max})\sum_{k=1}^K w_k^2\Big) < 1. \tag{25}
$$

This inequality requires $1 - \kappa\rho_{\max} > 0$, i.e., $\rho_{\max} < 1/\kappa$, and under this condition it is equivalent to

$$
\sum_{k=1}^K w_k^2 < \frac{1 - \kappa\rho_{\max}}{\kappa(1 - \rho_{\max})}. \tag{26}
$$

Using $K_{\mathrm{eff}} = 1/\sum_{k=1}^K w_k^2$, we obtain (21).

The bound improves when branches are less correlated (small $\rho_{\max}$) and the weights are not overly concentrated (large K_{eff}). In practice, the learning-to-rank module suppresses unreliable branches, which helps uncertainty reduction. The module's weights do not collapse onto a few branches, and different augmentations capture different knowledge, leading to weak inter-branch correlations. As a result, the conditions for uncertainty reduction are approximately satisfied in practice, which in turn improves transferability under domain shift.

V. EXPERIMENTS

This section details the experiments that verified the effectiveness of BFT on EEG datasets. All algorithms were implemented in Python, and the code is available on GitHub[1].

A. Datasets

A total of five EEG datasets under non-invasive collection devices were used in the experiments. Table I summarizes the main characteristics of the datasets.

Three motor imagery (MI) EEG datasets were used under classification tasks. Subjects were asked to perform imagined body part movements for a few seconds, and their EEG signals were recorded. Different types of imagination can be differentiated through the corresponding spatial sensorimotor rhythm modulations for BCI control. Left and right hand imagery tasks were considered.

Two driver-drowsiness estimation EEG datasets were used under regression tasks. EEG signals are used to estimate fatigue levels during driving (often simulated). Variations in neural patterns, such as increased theta or decreased alpha activity, reflect reduced vigilance [4], [29]. For measuring fatigue levels of the subjects, reaction time was converted to drowsiness index [30] for the Driving dataset, while PERCLOS [31] was used for the SEED-VIG dataset. Both metrics range in $[0, 1]$, with their calculation formulas available in the aforementioned publications. Thus, no further label normalization was applied.

---

[1] https://anonymous.4open.science/r/BFT-95C8/

TABLE I
SUMMARY OF THE FIVE EEG DATASETS.

Dataset	Number of Subjects	Number of Channels	Sampling Rate (Hz)	Trial Length (seconds)	Number of Trials	Task Type
Zhou2016 [32]	4	14	250	5	[90, 119]	left / right hand MI classification
BNCI2014001 [33]	9	22	250	4	144	left / right hand MI classification
HighGamma [34]	14	128	500	4	[160, 448]	left / right hand MI classification
Driving [35]	15	30	250	8	[1015, 1197]	reaction time (in drowsiness index) [0, 1] regression
SEED-VIG [36]	23	17	200	8	885	PERCLOS [0, 1] regression

B. Experiment Settings

We considered a plug-and-play evaluation setting under leave-one-subject-out cross-validation. For each experiment, one subject's data was held out as the test set, while data from the remaining subjects were combined as the training set. No information from the test set was accessible during the training phase, and the test phase was conducted using ordered trial-wise online data streams. Only the first session data were used to focus the study on inter-subject discrepancies.

All experiments were repeated three times with different random seeds. Since the used datasets contained many subjects, we report dataset-wise averaged performance scores (except for Zhou2016, which reported subject-wise scores), with standard deviations of variations across repeated experiments.

Classification performance was evaluated using accuracy, while regression performance was evaluated using the Pearson correlation coefficient (CC) and root mean squared error (RMSE) metrics.

To mitigate marginal distribution shift, we employed EA [9], [14] and BN-adapt [12], which are effective, backpropagation-free, and computationally efficient. These methods were integrated into all TTA approaches.

The backbone architecture used was EEGNet [37], a lightweight convolutional neural network architecture for EEG decoding. g is the convolution layers of EEGNet, h a fully-connected layer. τ was set to 0.5.

The ranking module $r(\cdot)$ is a fully-connected layer, whereas the mapping module $m(\cdot)$ is a bi-directional long short-term memory [38] network and a fully-connected layer. For training the mapping module, we followed [27] to generate synthetic samples $\mathcal{D}_{\text{synthetic}}$:

1) A uniform distribution over the interval $[-1, 1]$;
2) A normal distribution with mean $\mu = 0$ and standard deviation $\sigma = 1$;
3) A sequence of evenly spaced numbers within an uniformly drawn random sub-range of $[-1, 1]$;
4) Random mixtures of the above distributions.

C. EEG Transformations

The following transformations were applied to EEG trials during the experiments, most of which were introduced in Section III-B. To accommodate the sliding window augmentation, all other transformations operated on a truncated version of the trial, specifically the first $t - 1$ seconds, where t denotes the original trial duration in seconds. That is, the model input length for all transformations is $t - 1$ seconds. Given

the relatively long trial durations in the datasets used, this truncation has a negligible impact on performance. Moreover, the sliding window augmentation helps compensate for the discarded segment and further improves overall performance.

1) Identity: The original test trial is used without modification.
2) Amplitude Scaling (Scale): Each trial is scaled by one of the following factors: $[0.9, 1.1, 1.2]$.
3) Noise Addition (Noise): Gaussian noise proportional to the signal magnitude of each channel is added.
4) Frequency Shift (Freq): Low- and high-frequency components are selectively shifted.
5) Sliding Window (Slide): Five temporal segments of duration $t - 1$ are cropped from the full-length trial: $[0.2, t-0.8]$, $[0.4, t-0.6]$, $[0.6, t-0.4]$, $[0.8, t-0.2]$, and $[1, t]$. These windows simulate variations in signal onset. Unlike the other transformations, the sliding window operates on the untruncated trial.
6) Channel Reflection [39] and Discrete Wavelet Transform Augmentation [40]: These enhancements are label-aware transformations, and thus are applied only during training to improve the performance of the task module $h(g(\cdot))$ in classification tasks.

In total, fourteen transformations were used during training for classification tasks and twelve for regression tasks. On-the-fly augmentation was adopted, where each training sample was randomly transformed using one of the augmentation techniques with equal probability in each epoch. During test-time transformations in BFT-A, $K = 12$ types of transformations were applied to each test trial. $K = 10$ was used for BFT-D.

D. Results for Classification Task

The following approaches were evaluated, with descriptions and references of baselines available in [9].

1) CSP-LDA: Constructs Common Spatial Pattern filters followed by feature extraction and Linear Discriminant Analysis. Repeated experiments used 5, 6, and 7 CSP filters.
2) EEGNet: The baseline backbone trained using cross-entropy loss with or without data augmentation. The augmented version serves as the pretrained source models for all TTA methods to ensure fair comparison.
3) UDA: Includes DAN, DANN, CDAN-E, MDD, MCC, and SHOT-IM.
4) TTA with backpropagation: Includes MEMO, Tent, PL, SAR, and T-TIME.

5) TTA without backpropagation: Includes BN-adapt, T3A, and LAME.
6) Transformation-based TTA: Includes individual transformations of Aug-Scale, Aug-Noise, Aug-Freq, and Aug-Slide with results averaged across hyperparameter settings. We also report unweighted inference aggregation using MC Dropout and Aug-Mean as ablation baselines for BFT-D and BFT-A, respectively.

Results on the three MI EEG datasets are summarized in Tables II–III. Key observations include:

1) UDA approaches significantly outperformed baselines without TL. TTA with backpropagation achieved comparable, though slightly lower, gains, confirming the importance of TL in cross-subject EEG decoding.
2) Individual test-time transformations were unstable, as each type does not consistently improve performance. Aggregated inference of MC Dropout and Aug-Mean yielded more stable results, supporting the theoretical analysis in Section IV.
3) BFT-A consistently outperformed other backpropagation-free TTA approaches, whose performance was similar to that of T-TIME, the strongest backpropagation-based TTA approach. BFT-D also performed well, despite not relying on predefined transformations. Compared to naïve averaging of MC Dropout or Aug-Mean, both BFT variants benefited from the proposed learning-to-rank module in Section III-C.
4) The results verified that backpropagation-free TTA can be both effective and efficient, validating BFT-A/D as viable solutions for lightweight, plug-and-play BCIs.

TABLE II
SUBJECT-WISE CROSS-SUBJECT BINARY CLASSIFICATION ACCURACIES (%) ON ZHOU2016 MI EEG DATASET. THE BEST SCORES FOR EACH CATEGORY ARE MARKED IN BOLD.

Category	Approach	S1	S2	S3	S4	Avg.
w/o TTA	CSP-LDA	72.55	77.33	88.00	82.22	$80.03_{\pm0.56}$
	EEGNet (w/o Aug.)	82.35	75.33	89.00	80.74	$81.86_{\pm0.98}$
	EEGNet	80.95	81.00	93.67	79.63	$\mathbf{83.81}_{\pm2.06}$
UDA	DAN	78.43	78.67	89.33	75.56	$80.50_{\pm2.02}$
	JAN	78.43	78.67	87.67	80.37	$81.29_{\pm2.50}$
	DANN	78.15	78.00	89.33	77.41	$80.72_{\pm0.83}$
	CDAN-E	78.43	78.00	89.67	82.96	$82.27_{\pm2.03}$
	MDD	78.71	77.67	90.67	74.81	$80.47_{\pm0.90}$
	MCC	82.91	81.67	93.00	90.00	$\mathbf{86.90}_{\pm0.23}$
	SHOT-IM	82.91	80.00	94.00	84.07	$85.25_{\pm1.47}$
TTA w/ BP	MEMO	81.79	82.33	94.00	81.11	$84.81_{\pm2.26}$
	Tent	80.39	76.67	93.00	81.11	$82.79_{\pm2.11}$
	PL	83.19	77.00	93.67	85.18	$84.76_{\pm2.32}$
	SAR	80.67	73.00	92.33	85.18	$82.80_{\pm0.96}$
	T-TIME	83.75	78.00	93.33	86.30	$\mathbf{85.35}_{\pm0.82}$
TTA w/o BP	BN-adapt	82.35	79.00	94.00	80.37	$83.93_{\pm1.34}$
	T3A	73.95	74.67	91.00	56.30	$73.89_{\pm1.71}$
	LAME	84.03	77.33	93.33	79.26	$83.49_{\pm1.31}$
	Aug-Scale	80.95	80.00	93.67	79.26	$83.47_{\pm1.44}$
	Aug-Noise	80.95	80.67	92.67	80.00	$83.57_{\pm1.59}$
	Aug-Freq	80.95	80.33	93.67	80.37	$83.83_{\pm2.62}$
	Aug-Slide	82.35	77.33	93.00	80.37	$83.26_{\pm0.88}$
	MC Dropout	80.95	81.00	93.67	79.63	$83.81_{\pm2.06}$
	Aug-Mean	82.91	78.00	93.67	80.37	$83.74_{\pm2.67}$
	BFT-D (ours)	82.63	79.33	93.33	82.22	$84.38_{\pm1.22}$
	BFT-A (ours)	84.03	78.00	94.33	84.08	$\mathbf{85.11}_{\pm1.27}$

TABLE III
DATASET-WISE CROSS-SUBJECT BINARY CLASSIFICATION ACCURACIES (%) ON BNCI2014001 AND HIGHGAMMA MI EEG DATASET. THE BEST SCORES FOR EACH CATEGORY ARE MARKED IN BOLD.

Category	Approach	BNCI2014001	HighGamma
w/o TL	CSP-LDA	$72.76_{\pm0.31}$	$67.46_{\pm1.02}$
	EEGNet (w/o Aug.)	$75.39_{\pm1.22}$	$74.03_{\pm0.61}$
	EEGNet	$\mathbf{76.49}_{\pm0.45}$	$\mathbf{77.55}_{\pm0.26}$
UDA	DAN	$77.24_{\pm0.98}$	$75.42_{\pm0.88}$
	JAN	$74.90_{\pm1.11}$	$74.04_{\pm0.10}$
	DANN	$75.59_{\pm1.73}$	$75.41_{\pm1.05}$
	CDAN-E	$78.76_{\pm1.66}$	$73.94_{\pm0.46}$
	MDD	$76.44_{\pm1.10}$	$75.43_{\pm0.16}$
	MCC	$\mathbf{79.91}_{\pm1.12}$	$66.25_{\pm0.97}$
	SHOT-IM	$79.22_{\pm0.27}$	$\mathbf{77.72}_{\pm0.47}$
TTA w/ BP	MEMO	$76.80_{\pm0.37}$	$\mathbf{78.19}_{\pm0.34}$
	Tent	$74.56_{\pm1.29}$	$71.61_{\pm1.73}$
	PL	$77.13_{\pm1.55}$	$76.00_{\pm1.84}$
	SAR	$77.37_{\pm0.48}$	$71.64_{\pm2.00}$
	T-TIME	$\mathbf{79.22}_{\pm0.80}$	$77.42_{\pm0.76}$
TTA w/o BP	BN-adapt	$76.94_{\pm0.43}$	$78.23_{\pm0.45}$
	T3A	$69.75_{\pm3.45}$	$61.10_{\pm1.40}$
	LAME	$75.41_{\pm1.09}$	$77.74_{\pm0.35}$
	Aug-Scale	$76.34_{\pm0.38}$	$77.56_{\pm0.40}$
	Aug-Noise	$76.21_{\pm0.51}$	$77.72_{\pm0.23}$
	Aug-Freq	$76.13_{\pm1.13}$	$77.21_{\pm0.70}$
	Aug-Slide	$69.81_{\pm1.62}$	$75.65_{\pm0.68}$
	MC Dropout	$76.52_{\pm0.48}$	$77.55_{\pm0.26}$
	Aug-Mean	$76.31_{\pm0.60}$	$78.09_{\pm0.68}$
	BFT-D (ours)	$77.47_{\pm0.54}$	$78.54_{\pm0.40}$
	BFT-A (ours)	$\mathbf{77.80}_{\pm0.96}$	$\mathbf{79.03}_{\pm0.43}$

E. Results for Regression Task

As noted, many of the TL approaches are only applicable for classification task. For regression task, TL approaches generally can only handle marginal distribution shift, whereas conditional distribution shift is equally important but missing appropriate measures.

As noted, most TL approaches are designed for classification tasks, whereas only a few are applicable or design for regression tasks. The following approaches were evaluated:

1) PSD-MLP [30]: Extracts Power Spectral Density features and uses Multi-Layer Perceptron regressor.
2) EEGNet: Now trained using the MSE loss.
3) UDA: Includes DAN, DANN, CORAL, and DARE-GRAM [41].
4) TTA for regression: To our knowledge, few approaches have been proposed for TTA in regression. We compare against test-time transformations.

Results on the two driver-drowsiness EEG datasets are summarized in Tables IV. The absolute performance improvement was smaller in magnitude, yet the observations and conclusions are similar to the previous subsection.

F. Test-Time Robustness

This subsection investigates the robustness of TTA approaches to unexpected test-time noise. As discussed in Section II-C, practical EEG-based BCIs inevitably encounter signal contamination that degrades the quality of test samples. These artifacts of corruptions can be categorized into two

TABLE IV
DATASET-WISE CROSS-SUBJECT REGRESSION CCs AND RMSEs ON TWO DRIVER DROWSINESS ESTIMATION EEG DATASET. THE BEST SCORES FOR EACH CATEGORY ARE MARKED IN BOLD.

Category	Approach	Driving		SEED-VIG	
		CC ↑	RMSE ↓	CC ↑	RMSE ↓
w/o TL	PSD-MLP	$0.345_{\pm 0.033}$	$0.546_{\pm 0.083}$	$0.373_{\pm 0.007}$	$0.331_{\pm 0.049}$
	EEGNet (w/o Aug.)	$\mathbf{0.516}_{\pm 0.011}$	$\mathbf{0.275}_{\pm 0.001}$	$\mathbf{0.618}_{\pm 0.002}$	$0.225_{\pm 0.004}$
	EEGNet	$0.504_{\pm 0.017}$	$0.276_{\pm 0.004}$	$0.618_{\pm 0.006}$	$\mathbf{0.223}_{\pm 0.003}$
UDA	DAN	$0.522_{\pm 0.018}$	$0.272_{\pm 0.008}$	$0.609_{\pm 0.011}$	$0.216_{\pm 0.003}$
	DANN	$0.530_{\pm 0.008}$	$0.269_{\pm 0.006}$	$\mathbf{0.612}_{\pm 0.008}$	$0.213_{\pm 0.003}$
	CORAL	$\mathbf{0.531}_{\pm 0.005}$	$\mathbf{0.264}_{\pm 0.003}$	$0.611_{\pm 0.006}$	$\mathbf{0.209}_{\pm 0.003}$
	DARE-GRAM	$0.511_{\pm 0.008}$	$0.275_{\pm 0.008}$	$0.609_{\pm 0.009}$	$0.215_{\pm 0.003}$
TTA w/o BP	BN-adapt	$0.526_{\pm 0.010}$	$0.278_{\pm 0.008}$	$0.618_{\pm 0.010}$	$0.216_{\pm 0.004}$
	Aug-Scale	$0.506_{\pm 0.018}$	$0.275_{\pm 0.004}$	$0.619_{\pm 0.005}$	$0.223_{\pm 0.003}$
	Aug-Noise	$0.502_{\pm 0.016}$	$0.275_{\pm 0.003}$	$0.618_{\pm 0.006}$	$0.222_{\pm 0.002}$
	Aug-Freq	$0.504_{\pm 0.017}$	$0.276_{\pm 0.005}$	$0.617_{\pm 0.006}$	$0.223_{\pm 0.002}$
	Aug-Slide	$0.504_{\pm 0.018}$	$0.276_{\pm 0.004}$	$0.618_{\pm 0.004}$	$0.223_{\pm 0.003}$
	MC Dropout	$0.504_{\pm 0.017}$	$0.278_{\pm 0.004}$	$0.618_{\pm 0.006}$	$0.218_{\pm 0.001}$
	Aug-Mean	$0.510_{\pm 0.017}$	$0.277_{\pm 0.001}$	$0.625_{\pm 0.005}$	$0.222_{\pm 0.003}$
	BFT-D (ours)	$0.534_{\pm 0.009}$	$0.272_{\pm 0.005}$	$0.623_{\pm 0.007}$	$\mathbf{0.207}_{\pm 0.002}$
	BFT-A (ours)	$\mathbf{0.535}_{\pm 0.008}$	$\mathbf{0.271}_{\pm 0.006}$	$\mathbf{0.629}_{\pm 0.005}$	$0.208_{\pm 0.002}$

broad types, which we simulate and inject into test trials, as shown in Fig. 5:

1) Temporal noise, resulting from factors such as body movements. To simulate this, Gaussian noise was added to the temporal segment between $[1.5, 2.0]$ seconds of each test trial, with variance proportional to the signal magnitude for each channel.

2) Spatial noise, resulting from poor electrode-skin contact, etc. This is simulated by injecting Gaussian noise again into a single random channel over the entire trial duration, with variance proportional to the signal magnitude of that specific channel.

These noise/corruptions can also be regarded as transformation functions; however, unlike the aforementioned semantic-preserving transformations, these noise may not preserve the semantics of the original task label.

The results are presented in Fig. 6 and Fig. 7. Observe that:

1) For temporal noise, BFT-D/A maintained its original performance across all five datasets, while the baseline and other TL approaches suffered different extents of performance drop.

2) For spatial noise, all approaches suffered a performance drop in the absolute values of the metrics, along with significantly higher instability. Nevertheless, BFT-D/A still achieved the best performance in all cases. This indicates that spatial noise is more challenging to address, likely because the two paradigms depend heavily on spatial information, and the EEGNet architecture also emphasizes spatial information extraction.

G. Ablation Studies

We conducted ablation studies to validate the proposed learning-to-rank transformation module.

First, we analyzed whether the mapping module $m(\cdot)$ is necessary. We compared the following:

1) Variant 1: BFT with no $m(\cdot)$ module. The task loss for training samples was directly utilized to train $r(\cdot)$. The inverse of the outputs of $r(\cdot)$ were used as reliability scores for aggregation.

2) Variant 2: BFT with no $m(\cdot)$ module. The task loss for training samples was directly utilized to train $r(\cdot)$. The inverse of the outputs of $r(\cdot)$ were converted to integer ranks, and then used as reliability scores for aggregation.

3) BFT with full $r(\cdot)$ and $m(\cdot)$ modules.

The results are shown in Table V. Observe that the last strategy generally yielded the best or the most stable performance with less standard deviation, indicating the necessity of the mapping module.

TABLE V
SUBJECT-WISE CROSS-SUBJECT BINARY CLASSIFICATION ACCURACIES (%) ON ZHOU2016 MI EEG DATASET.

Category	Approach	S1	S2	S3	S4	Avg.
Variant 1	BFT-D	82.63	79.00	93.67	82.59	$\mathbf{84.47}_{\pm 2.28}$
	BFT-A	83.75	77.67	93.67	83.33	$84.60_{\pm 2.56}$
Variant 2	BFT-D	82.35	79.33	93.67	81.85	$84.30_{\pm 2.33}$
	BFT-A	83.75	77.33	93.00	82.59	$84.17_{\pm 2.33}$
BFT	BFT-D	82.62	79.33	93.33	82.22	$84.38_{\pm 1.22}$
	BFT-A	84.03	78.00	94.33	84.08	$\mathbf{85.11}_{\pm 1.27}$

Additional results for ablation studies for classification and regression tasks are presented in Fig. 8.

In Fig. 8(a) for classification tasks, across different transformations of the test samples, those with lower task losses generally received higher reliability weights, although the magnitude differences were often subtle. The rank-based conversion amplified these distinctions, leading to more clearly separated aggregation weights. This observation confirms that the mapping module $m(\cdot)$ is essential for addressing the limitations discussed in Section III-C.
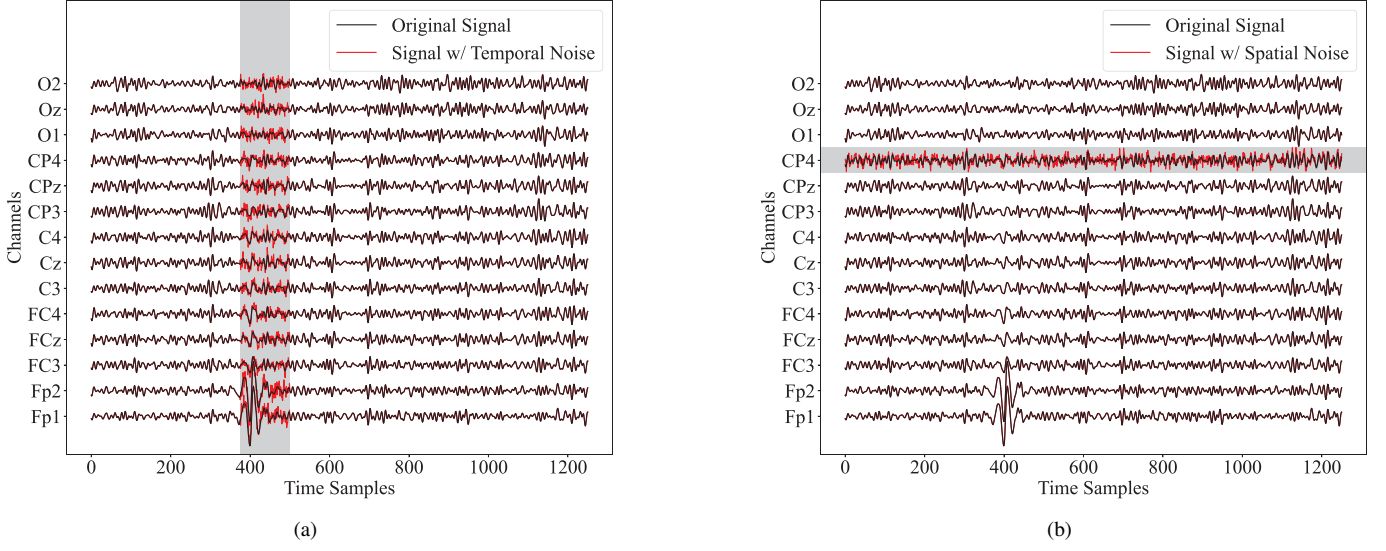
Fig. 5. Two types of test-time noise, using an EEG trial from Zhou2016 as an example. (a) temporal noise; and (b) spatial noise.
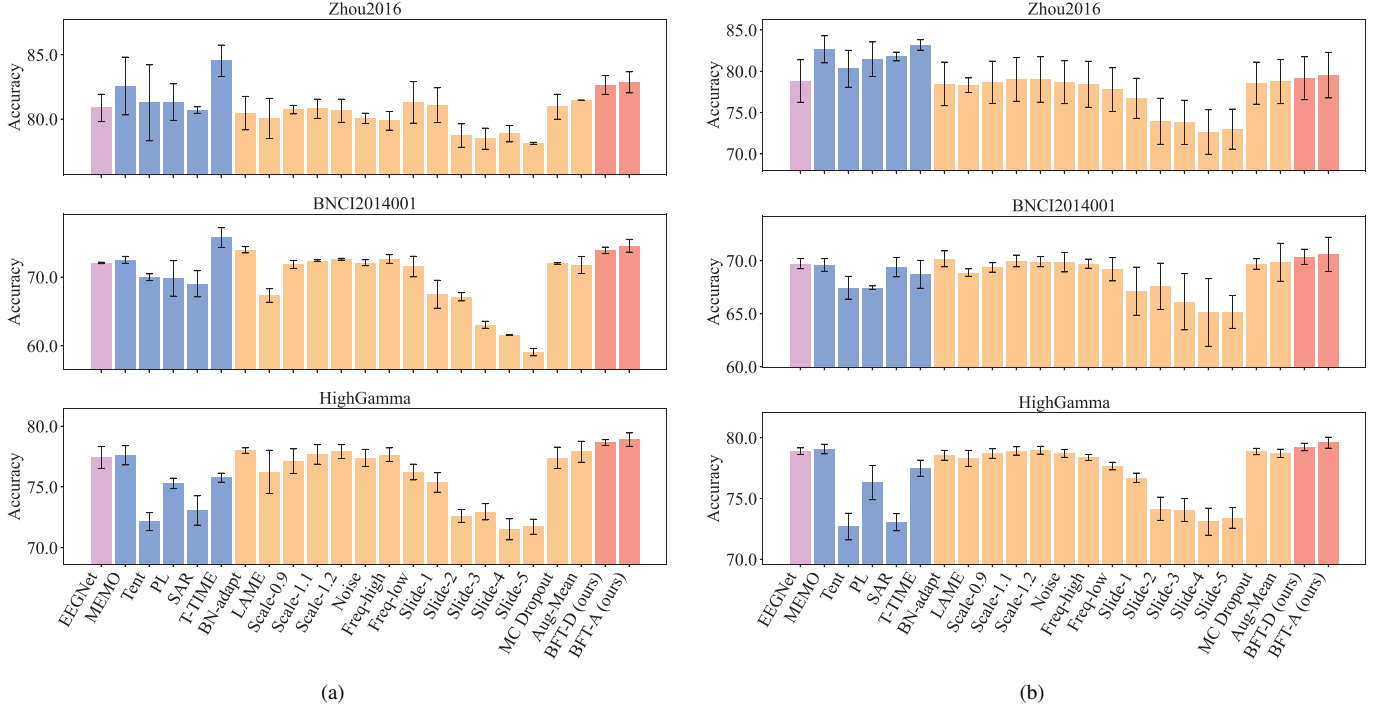

Fig. 6. Accuracy (%) under temporal and spatial noise during test phase for the three MI classification datasets. (a) temporal noise; and (b) spatial noise.

In Fig. 8(b) for regression tasks, the ranking module achieved a median Normalized Discounted Cumulative Gain (NDCG) score of 0.611 across test trials, considering the top half of the twelve transformations. Although the variation across trials was substantial, the performance remained substantially better than random ranking. Interestingly, we empirically observed that the ranking module's outputs slightly outperformed those of the mapping module.

It should be noted that the outputs of $m(\cdot)$ are not directly employed in aggregation for either classification or regression, as illustrated in Fig. 3. Instead, the effectiveness of $m(\cdot)$ arises from its projection into a rank-like space, combined with the $L1$ loss objective, which regularizes the learning of the ranking module $r(\cdot)$. This mechanism enables $r(\cdot)$ to produce more discriminative reliability scores across transformations, enabling more effective prediction aggregation.

These findings collectively demonstrate the effectiveness of the mapping and ranking modules in improving test-time performance.
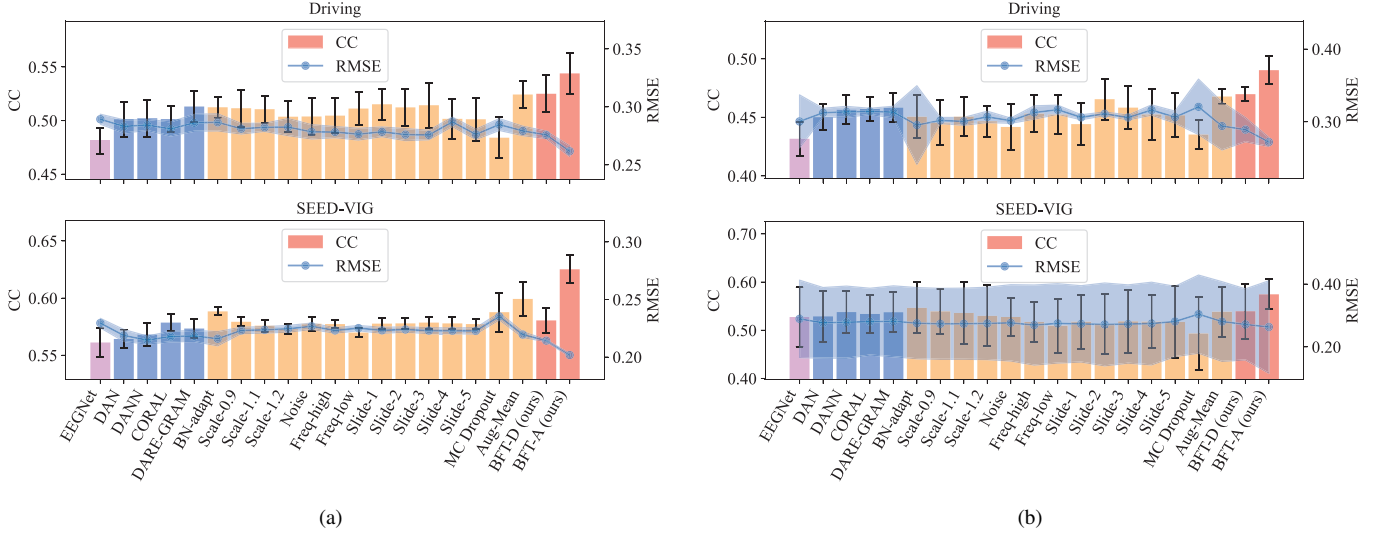
Fig. 7. CCs and RMSEs under temporal and spatial noise during test phase for the two driver-drowsiness regression datasets. (a) temporal noise; and (b) spatial noise.
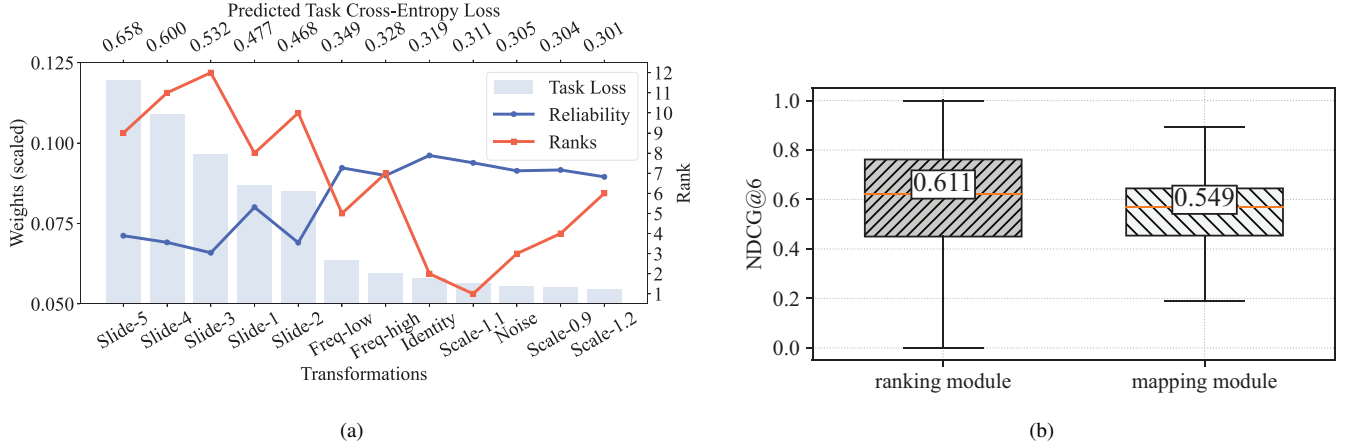

Fig. 8. Evaluation of the learning-to-rank module for aggregation in classification and regression tasks. (a) Using subject S1 from the BNCI2014001 dataset as an example, three metrics were computed and averaged over all test trials for each of the twelve BFT-A transformations: (1) cross-entropy loss from the classifier $h(\cdot)$, (2) reliability weights from the ranking module $r(\cdot)$, and (3) integer-like ranks from the mapping module $m(\cdot)$. All weights were normalized to sum up to one; and (b) Using subject S1 from the Driving dataset as the test set as an example, we compared the statistics of NDCG@6, as the metric of the ranking performance of the reliability of the top-half of the transformations between: (1) ranking module's outputs, against the ground-truth task MSE loss; and (2) mapping module's outputs, against the ground-truth task MSE loss.

H. Quantization for Deployment

In practice, neural network models for decoding in BCIs must operate under strict latency and memory constraints for edge computing [42], [43]. Therefore, model quantization should be widely adopted to reduce computational cost and storage space while enabling faster real-time inference [19], [44]. We evaluated under reduced precision by applying post-training static quantization [18]. Specifically, model weights trained on the source data were converted from 32-bit floating-point to 8-bit integer precision, using the training data. We tested the model on an NVIDIA GeForce RTX 3090 GPU and an Intel(R) Xeon(R) Platinum 8176 CPU.

The results shown in Table VI demonstrate that our proposed BFT approaches consistently retained the decoding performance improvements even after quantization. This suggests that BFT is lightweight and fully compatible with quantized models, making it suitable for resource-constrained deployment scenarios.

Regarding computation time, the overall computation time in a practical BCI decoding pipeline can be decomposed into the following components:

1) EEG preprocessing: Typically includes band-pass filtering, artifact removal, etc. Since this part depends heavily on the acquisition hardware and EEG processing software, it is not included in our measurements.
2) EA: Multiplying the test trial by the target mean covariance reference matrix, in addition to incrementally updating the reference matrix online [9], requires only ∼3 ms. This step is essential for mitigating marginal distribution shift.

TABLE VI
DATASET-WISE CROSS-SUBJECT BINARY CLASSIFICATION ACCURACIES
(%) ON ZHOU2016.

Quantization	Device	Approach	Performance
No	GPU	EEGNet	$80.95_{\pm2.77}$
Yes	CPU	EEGNet	$80.95_{\pm2.10}$
No	GPU	T-TIME	$83.75_{\pm0.40}$
Yes	CPU	T-TIME	N/A
No	GPU	BFT-A	$84.03_{\pm2.74}$
Yes	CPU	BFT-A	$83.19_{\pm3.43}$
No	GPU	BFT-D	$82.63_{\pm2.21}$
Yes	CPU	BFT-D	$82.07_{\pm0.79}$

3) Transformations: Constructing the transformations as discussed in Sect. V-C requires ∼4 ms for BFT-A. BFT-D has no extra computations for constructing transformations.

4) Forward pass: On GPU, forward pass requires < 1 ms. On CPU, it takes ∼2 ms for 32-bit float models. Note that the Intel CPU used in our experiments does not directly support advanced integer acceleration instructions such as Advanced RISC Machines [45] architecture with dedicated integer dot-product units. Ideally, under such proper processing device for BCIs, inference latency for quantized models can be further significantly lowered due to optimized 8-bit integer kernels [19].

5) Backward pass: Updating model parameters through backpropagation requires ∼5 ms on GPU but more than 50 ms on CPU. Importantly, quantization generally limits the applicability of backpropagation due to reduced precision, making backpropagation-based TTA approaches not suitable in quantized deployments.

In summary, our proposed BFT framework is well-suited to the practical requirements of BCI deployment. It achieves real-time adaptation with minimal overhead, preserves the benefits of quantization for efficient inference, and remains fully compatible with edge device deployment.

VI. CONCLUSIONS

This paper proposed a BFT approach that performs sample-wise prediction refinement during deployment, effectively reducing inference uncertainty. BFT is lightweight, having advantages of backpropagation-free, privacy-preserving, noise-robust, task-agnostic.

Our future research includes:

1) Label distribution shift: Addressing label distribution shift remains particularly challenging without access to labeled target domain data. Only a few approaches are applicable in this setting, and further investigation is needed.

2) Asynchronous TL: Adapting to asynchronous BCIs, where the onset of trials is not explicitly marked, remains an open problem.

3) Trial rejection: Incorporating out-of-distribution detection to identify and reject unreliable or corrupted test samples is a promising direction.

REFERENCES

[1] X. Gao, Y. Wang, X. Chen, and S. Gao, "Interface, interaction, and intelligence in generalized brain–computer interfaces," *Trends in Cognitive Sciences*, vol. 25, no. 8, pp. 671–684, 2021.

[2] D. Wu, X. Jiang, and R. Peng, "Transfer learning for motor imagery based brain-computer interfaces: A tutorial," *Neural Networks*, vol. 153, pp. 235–253, 2022.

[3] D. Wu, B.-L. Lu, B. Hu, and Z. Zeng, "Affective brain–computer interfaces (aBCIs): A tutorial," *Proc. of the IEEE*, vol. 111, no. 10, pp. 1314–1332, 2023.

[4] B. Fu, F. Boutros, C.-T. Lin, and N. Damer, "A survey on drowsiness detection: Modern applications and methods," *IEEE Trans. Intelligent Vehicles*, vol. 9, no. 11, pp. 7279–7300, 2024.

[5] C. Vidaurre, A. Schlogl, R. Cabeza, R. Scherer, and G. Pfurtscheller, "A fully on-line adaptive BCI," *IEEE Trans. Biomedical Engineering*, vol. 53, no. 6, pp. 1214–1219, 2006.

[6] F. Zhuang, Z. Qi, K. Duan, D. Xi, Y. Zhu, H. Zhu, H. Xiong, and Q. He, "A comprehensive survey on transfer learning," *Proc. of the IEEE*, vol. 109, no. 1, pp. 43–76, 2021.

[7] J. Liang, R. He, and T. Tan, "A comprehensive survey on test-time adaptation under distribution shifts," *Int'l Journal of Computer Vision*, vol. 133, pp. 31–64, 2025.

[8] Z. Wang, Y. Luo, L. Zheng, Z. Chen, S. Wang, and Z. Huang, "In search of lost online test-time adaptation: A survey," *Int'l Journal of Computer Vision*, vol. 133, p. 1106–1139, 2024.

[9] S. Li, Z. Wang, H. Luo, L. Ding, and D. Wu, "T-TIME: Test-time information maximization ensemble for plug-and-play BCIs," *IEEE Trans. Biomedical Engineering*, vol. 71, no. 2, pp. 423–432, 2024.

[10] J. Lu, A. Liu, F. Dong, F. Gu, J. Gama, and G. Zhang, "Learning under concept drift: A review," *IEEE Trans. Knowledge and Data Engineering*, vol. 31, no. 12, pp. 2346–2363, 2019.

[11] Z. Xiao and C. G. Snoek, "Beyond model adaptation at test time: A survey," *arXiv preprint arXiv:2411.03687*, 2024.

[12] S. Schneider, E. Rusak, L. Eck, O. Bringmann, W. Brendel, and M. Bethge, "Improving robustness against common corruptions by covariate shift adaptation," in *Proc. Advances in Neural Information Processing Systems*, Vancouver, Canada, Dec. 2020, pp. 11 539–11 551.

[13] D. Wang, E. Shelhamer, S. Liu, B. Olshausen, and T. Darrell, "Tent: Fully test-time adaptation by entropy minimization," in *Int'l Conf. Learning Representations*, Vienna, Austria, May. 2021.

[14] H. He and D. Wu, "Transfer learning for brain-computer interfaces: A Euclidean space data alignment approach," *IEEE Trans. Biomedical Engineering*, vol. 67, no. 2, pp. 399–410, 2020.

[15] D.-H. Lee, "Pseudo-Label: The simple and efficient semi-supervised learning method for deep neural networks," in *Proc. Int'l Conf. Machine Learning Workshops*, Atlanta, GA, Jun. 2013, pp. 1322–1333.

[16] S. Niu, J. Wu, Y. Zhang, Z. Wen, Y. Chen, P. Zhao, and M. Tan, "Towards stable test-time adaptation in dynamic world," in *Int'l Conf. Learning Representations*, Kigali, Rwanda, May. 2023.

[17] M. M. Zhang, S. Levine, and C. Finn, "MEMO: Test time robustness via adaptation and augmentation," in *Proc. Advances in Neural Information Processing Systems*, New Orleans, LA, Nov. 2022, pp. 38 629–38 642.

[18] B. Jacob, S. Kligys, B. Chen, M. Zhu, M. Tang, A. Howard, H. Adam, and D. Kalenichenko, "Quantization and training of neural networks for efficient integer-arithmetic-only inference," in *Proc. IEEE Conf. Computer Vision and Pattern Recognition*, Salt Lake City, UT, Jun. 2018, pp. 2704–2713.

[19] T. Schneider, X. Wang, M. Hersche, L. Cavigelli, and L. Benini, "Q-EEGNet: an energy-efficient 8-bit quantized parallel EEGNet implementation for edge motor-imagery brain-machine interfaces," in *Proc. IEEE Int'l Conf. Smart Computing*, Bologna, Italy, Sep. 2020, pp. 284–289.

[20] K. Xia, W. Duch, Y. Sun, K. Xu, W. Fang, H. Luo, Y. Zhang, D. Sang, X. Xu, F.-Y. Wang, and D. Wu, "Privacy-preserving brain–computer interfaces: A systematic review," *IEEE Trans. Computational Social Systems*, vol. 10, no. 5, pp. 2312–2324, 2023.

[21] A. Dionysiou, V. Vassiliades, and E. Athanasopoulos, "Exploring model inversion attacks in the black-box setting," in *Proc. Privacy Enhancing Technologies*, Washington, DC, Jul. 2023, pp. 190–206.

[22] H. Zhao, Y. Liu, A. Alahi, and T. Lin, "On pitfalls of test-time adaptation," in *Proc. Int'l Conf. Machine Learning*, Honolulu, HI, Jul. 2023.

[23] W. Zhang, L. Deng, L. Zhang, and D. Wu, "A survey on negative transfer," *IEEE/CAA Journal of Automatica Sinica*, vol. 10, no. 2, pp. 305–329, 2023.

[24] D. Freer and G.-Z. Yang, "Data augmentation for self-paced motor imagery classification with C-LSTM," *Journal of Neural Engineering*, vol. 17, no. 1, p. 016041, 2020.

[25] Y. Gal and Z. Ghahramani, "Dropout as a Bayesian approximation: Representing model uncertainty in deep learning," in *Proc. Int'l Conf. Machine Learning*, New York City, NY, Jun. 2016, pp. 1050–1059.

[26] T.-Y. Liu *et al.*, "Learning to rank for information retrieval," *Foundations and Trends in Information Retrieval*, vol. 3, no. 3, pp. 225–331, 2009.

[27] M. Engilberge, L. Chevallier, P. Pérez, and M. Cord, "SoDeep: a sorting deep net to learn ranking loss surrogates," in *Proc. IEEE/CVF Conf. Computer Vision and Pattern Recognition*, Long Beach, CA, Jun. 2019, pp. 10 792–10 801.

[28] Z.-H. Zhou, *Ensemble Methods: Foundations and Algorithms*. CRC Press, 2012.

[29] G. Du, S. Long, C. Li, Z. Wang, and P. X. Liu, "A product fuzzy convolutional network for detecting driving fatigue," *IEEE Trans. Cybernetics*, vol. 53, no. 7, pp. 4175–4188, 2023.

[30] Y. Cui, Y. Xu, and D. Wu, "EEG-based driver drowsiness estimation using feature weighted episodic training," *IEEE Trans. Neural Systems and Rehabilitation Engineering*, vol. 27, no. 11, pp. 2263–2273, 2019.

[31] W. W. Wierwille and L. A. Ellsworth, "Research on vehicle-based driver status/performance monitoring: Development, validation, and refinement of algorithms for detection of driver drowsiness. final report," U.S. Department of Transportation, National Highway Traffic Safety Administration, Tech. Rep. DOT HS 808 247, 1994.

[32] B. Zhou, X. Wu, Z. Lv, L. Zhang, and X. Guo, "A fully automated trial selection method for optimization of motor imagery based brain-computer interface," *PloS One*, vol. 11, no. 9, p. e0162657, 2016.

[33] M. Tangermann, K.-R. Müller, A. Aertsen, N. Birbaumer, C. Braun, C. Brunner, R. Leeb, C. Mehring, K. J. Miller, G. R. Müller-Putz *et al.*, "Review of the BCI competition IV," *Frontiers in Neuroscience*, vol. 6, p. 55, 2012.

[34] R. T. Schirrmeister, J. T. Springenberg, L. D. J. Fiederer, M. Glasstetter, K. Eggensperger, M. Tangermann, F. Hutter, W. Burgard, and T. Ball, "Deep learning with convolutional neural networks for EEG decoding and visualization," *Human Brain Mapping*, vol. 38, no. 11, pp. 5391–5420, 2017.

[35] C.-H. Chuang, L.-W. Ko, T.-P. Jung, and C.-T. Lin, "Kinesthesia in a sustained-attention driving task," *Neuroimage*, vol. 91, pp. 187–202, 2014.

[36] W.-L. Zheng and B.-L. Lu, "A multimodal approach to estimating vigilance using EEG and forehead EOG," *Journal of Neural Engineering*, vol. 14, no. 2, p. 026017, 2017.

[37] V. J. Lawhern, A. J. Solon, N. R. Waytowich, S. M. Gordon, C. P. Hung, and B. J. Lance, "EEGNet: A compact convolutional neural network for EEG-based brain-computer interfaces," *Journal of Neural Engineering*, vol. 15, no. 5, p. 056013, 2018.

[38] S. Hochreiter and J. Schmidhuber, "Long short-term memory," *Neural Computation*, vol. 9, no. 8, pp. 1735–1780, 1997.

[39] Z. Wang, S. Li, J. Luo, J. Liu, and D. Wu, "Channel reflection: Knowledge-driven data augmentation for EEG-based brain–computer interfaces," *Neural Networks*, vol. 176, p. 106351, 2024.

[40] Z. Wang, S. Li, X. Chen, and D. Wu, "Time–frequency transform based EEG data augmentation for brain–computer interfaces," *Knowledge-Based Systems*, vol. 311, p. 113074, 2025.

[41] I. Nejjar, Q. Wang, and O. Fink, "DARE-GRAM: Unsupervised domain adaptation regression by aligning inverse GRAM matrices," in *Proc. IEEE/CVF Conf. Computer Vision and Pattern Recognition*, Vancouver, Canada, Jun. 2023, pp. 11 744–11 754.

[42] J.-H. Syu, J. C.-W. Lin, G. Srivastava, and K. Yu, "A comprehensive survey on artificial intelligence empowered edge computing on consumer electronics," *IEEE Trans. Consumer Electronics*, vol. 69, no. 4, pp. 1023–1034, 2023.

[43] J. Chen and X. Ran, "Deep learning with edge computing: A review," *Proc. of the IEEE*, vol. 107, no. 8, pp. 1655–1674, 2019.

[44] X. Wang, M. Hersche, B. Tömekce, B. Kaya, M. Magno, and L. Benini, "An accurate EEGNet-based motor-imagery brain–computer interface for low-power edge computing," in *IEEE Int'l Symposium on Medical Measurements and Applications*, Bari, Italy, Jul. 2020, pp. 1–6.

[45] L. Lai, N. Suda, and V. Chandra, "CMSIS-NN: Efficient neural network kernels for ARM Cortex-M CPUs," *arXiv preprint arXiv:1801.06601*, 2018.